

Clock-jitter reduction in LISA time-delay interferometry combinations

Olaf Hartwig

*Max-Planck-Institut für Gravitationsphysik (Albert-Einstein-Institut),
Callinstraße 38, 30167 Hannover, Germany*

Jean-Baptiste Bayle

*Jet Propulsion Laboratory, California Institute of Technology,
4800 Oak Grove Drive, Pasadena, CA 91109, USA*

(Dated: May 8, 2020)

The Laser Interferometer Space Antenna (LISA) is a European Space Agency mission that aims to measure gravitational waves in the millihertz range. The three-spacecraft constellation form a nearly-equilateral triangle, which experiences flexing along its orbit around the Sun. These time-varying and unequal armlengths require to process measurements with Time-Delay Interferometry (TDI) to synthesize a virtual equal-arm interferometer, and reduce the otherwise-overwhelming laser frequency noise. Algorithms compatible with such TDI combinations have recently been proposed in order to suppress the phase fluctuations of the onboard ultra-stable oscillators (USO) used as reference clocks.

In this paper, we present a method to compute improved algorithms, which provide exact cancellation of the USO noise for a large class of TDI combinations, even for time-varying armlengths, if we neglect Doppler effects. We account for errors present in the sideband signals used in the algorithm, and include a new step to reduce it. We propose analytic models for the power spectral densities of residual noises, including residual clock noise due to the filters used on board to downsample data before telemetry. We present the results of simulations, which include realistic USO noise. We show that our model agrees very well with the simulated data, and that our algorithms are able to reduce clock jitter well below other noises, and the mission requirements.

I. INTRODUCTION

The Laser Interferometer Space Antenna (LISA) is a European Space Agency (ESA) scientific space mission, which aims to measure gravitational waves (GWs) in the millihertz range [1]. Those waves are predicted by Einstein's theory of General Relativity and produced by the quadrupolar moment of very dense objects, such as black hole binaries, or coalescing super-massive black holes. The detection of low-frequency gravitational waves will help answer numerous astrophysical, cosmological, and theoretical questions. They are related, for example, to the formation of black hole binaries and extreme mass ratio inspirals, the formation of galaxies, or General Relativity in the strong field regime [1].

The mission is expected to be launched in the year 2034. Three spacecraft will trail the Earth around the Sun, in a nearly equilateral trian-

gular configuration with armlengths of about 2.5 million kilometers. Each spacecraft contains two free-falling test masses acting as inertial sensors [1], and two optical benches. Six laser links connect the six optical benches performing interferometric measurements between the local and distant laser beams. These optical setups are capable of measuring the differential acceleration between the local and remote test masses with sub-picometer precision [2, 3]. In the latest design, each spacecraft performs six interferometric measurements [4], which are then telemetered to Earth.

The dominant source of noise in LISA is laser frequency noise, which couples into the measurements many orders of magnitude above the expected gravitational wave signals. Time-delay interferometry (TDI) is an offline technique proposed by [5] to suppress this laser noise. It uses time-shifted combinations of the interferometric signals to synthesize virtual laser-noise-free Michelson-like interferometers. The so-called

first-generation algorithm assumes that the arm-lengths are constant in time. A second generation has been proposed, to account for flexing of the constellation [6], *i.e.* time-varying arm-lengths. The basic working principles of TDI have been demonstrated experimentally [7–10], and analytic and numerical studies [11–13] have shown that the second-generation TDI is sufficient to reduce laser noise below the required levels.

In addition to laser frequency noise, other secondary noise sources are also above the requirements and need to be suppressed as part of the TDI algorithm. In particular, this is envisioned for phase fluctuations of the ultra-stable oscillators on board each spacecraft.

One ultra-stable oscillator (USO) per spacecraft provides a unique time reference used to drive all systems of the onboard measurement chain. This clock drives in particular the analog-to-digital converter (ADC), the phasemeter, and the onboard computer. The same clock signal is also used to timestamp the measurements at 3 Hz, which are then telemetered down to Earth. To prevent aliasing below 1 Hz [14], the signals are filtered before they are downsampled.

State-of-the-art space-qualified oscillators typically have an Allan deviation of about 10^{-13} for averaging times above 1 s [15]. No active synchronization between the clocks is foreseen, such that timestamps of measurements from different spacecraft are inconsistent with each other. The drifting of the clocks also affect the pseudo-ranging measurements used to estimate the absolute distance between the spacecraft, themselves used to produce the TDI variables. In this study, we assume that an onground algorithm can synchronize the measurements onto a common time grid. This removes the clock offsets from the ranging measurement, such that we can ignore this effect on TDI [16].

In addition to timing and ranging errors due to drifts over large timescales, clock jitter in the measurement band also needs to be considered. It is much higher than the tolerable level to achieve the science objectives [REF?]. In order to suppress it, we imprint the clock reference signal onto the laser beam in form of modulation

sidebands. This allows an independent measurement of the differential clock jitter, which can be used for clock noise suppression algorithms. Technical details on the sideband generation can be found in [17].

A first version of such an algorithm for first-generation TDI was presented in [ref Tinto], which perfectly cancels clock noise assuming constant arm-lengths. In [18], it was shown that this algorithm can be extended for second-generation TDI, where it reduces the USO noise to far below other secondary noises. However, the cancellation has residuals due to the constellation flexing. In this article, we propose new algorithms for both generations, which are free of this residual noise. We use a generic formulation which is applicable to most second-generation TDI combinations.

We estimate the residual noise from the flexing-filtering effect first described in [13], as well as the level of other secondary noises. We show that numerical simulations match our analytic expressions.

In section II, we introduce the notations and conventions used in this article. Then, in section III, we give the equations for the interferometric measurements, and study how clock noise appear in the TDI variables. This allows us to propose a reduction algorithm in section IV, and compute the levels of the secondary noises in the corrected variables. We then present our simulation setup in section VI, before discussing the main results in section VII.

II. NOTATIONS AND CONVENTIONS

Various conventions are used in the literature to label the spacecraft, optical benches and light travel times along the links. In this paper, we number these components according to fig. 1. We consider the so-called *split-interferometry* optical layout, described in [4]. Therefore six interferometric measurements are formed on each spacecraft. They are indexed according to associated optical bench. We give here equations for the first spacecraft. The remaining expressions can be deduced by the circular permutation of

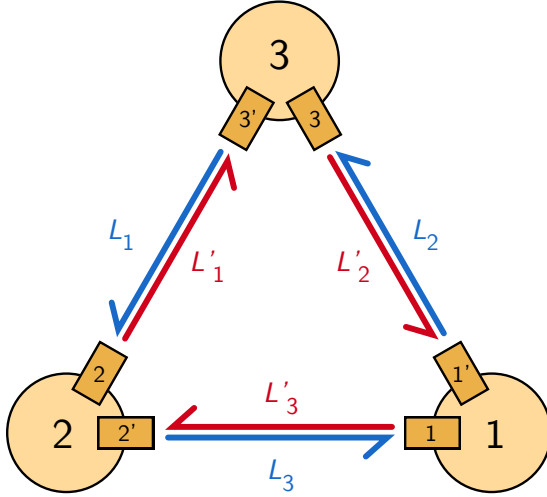


Figure 1. Indexing convention used in this paper. Optical benches, links and light travel times pointing counterclockwise are denoted with primed indices.

indices $1 \rightarrow 2 \rightarrow 3 \rightarrow 1$.

In the following, all interferometric signals are expressed in terms of absolute frequency deviations from the carrier frequency of the associated beam. Differences in the carrier frequencies are only considered for the calculation of the heterodyne beatnote frequencies, which we assume to be constant. They are defined as

$$a_1 = \nu_{2'} - \nu_1 \quad \text{and} \quad a_{1'} = \nu_3 - \nu_{1'}, \quad (1)$$

$$b_1 = \nu_{1'} - \nu_1 \quad \text{and} \quad b_{1'} = -b_1, \quad (2)$$

$$\begin{aligned} c_1 &= (\nu_{2'} + \nu_{2'}^m) - (\nu_1 + \nu_1^m) \\ &= a_1 + \nu_{2'}^m - \nu_1^m, \end{aligned} \quad (3)$$

$$\begin{aligned} c_{1'} &= (\nu_3 + \nu_3^m) - (\nu_{1'} + \nu_{1'}^m) \\ &= a_{1'} + \nu_3^m - \nu_{1'}^m, \end{aligned} \quad (4)$$

with $\nu_i \approx 282$ THz as the laser frequencies. The beatnote frequencies themselves fall into a range of ± 5 MHz to ± 25 MHz

The science and reference beatnote frequencies are denoted by a_i and b_i , and their signs are defined as θ_i^s and θ_i^r , respectively. The test-mass interferometers use the same beams as the reference interferometers, and therefore their beatnotes are at the same frequency b_i .

The sideband frequencies are offset by $\pm \nu_i^m = 2.4$ GHz and $\pm \nu_{i'}^m = 2.401$ GHz with respect to the carrier frequency. We only consider the upper sidebands for this study, and neglect the effect of Doppler shifts. Therefore, the sideband beatnote in the science interferometers are at $a_1 + (\nu_{2'}^m - \nu_1^m)$ and $a_{1'} + (\nu_3^m - \nu_{1'}^m)$, respectively, and thus offset by ± 1 MHz from the respective carrier beatnote¹. In addition, sideband beatnotes in the reference interferometers are observed at the frequencies $b_1 + (\nu_1^m - \nu_{1'}^m)$ and $b_{1'} + (\nu_{1'}^m - \nu_1^m)$.

We define $L_i(t)$ as the light travel time along link i , in seconds. The propagation of laser beams along this link is modeled using the time-varying delay operator \mathcal{D}_i , such that $\mathcal{D}_i x(t) = x(t - L_i(t))$ for any time-dependent function $x(t)$. Multiple delays use the short-hand notation

$$\mathcal{D}_{i_1} \mathcal{D}_{i_2} \dots \mathcal{D}_{i_n} \equiv \mathcal{D}_{i_1 i_2 \dots i_n}. \quad (5)$$

Since the delays $L_i(t)$ are themselves not constant, delay operators do not commute.

Anti-aliasing filters are used on board to down-sample the data. They consist of a convolution with the filter kernel $f(t)$. We can define the filter operator \mathcal{F} , such that $\mathcal{F}x(t) \equiv (f * x)(t)$.

We define

$$[\mathcal{F}, \mathcal{D}_i]x(t) = \mathcal{F}\mathcal{D}_i x(t) - \mathcal{D}_i \mathcal{F}x(t). \quad (6)$$

as the commutator of the filter operator with a delay. In [13], it is shown that these terms are non-vanishing and contribute to the residual noise.

If $x(t)$ is a function of time, we denote its Fourier transform $\tilde{x}(\omega)$ and its Power Spectral Density (PSD) $S_x(\omega)$, both functions of the angular frequency $\omega = 2\pi f$. For indexed quantities like *e.g.* clock noise, we assume that their PSDs are equal, and denote them by $S_q(\omega)$.

¹ The exact values given here are preliminary. What is important is that the sideband beatnotes end up at a different frequency than the carrier beatnotes, which enables to track their phases independently.

III. MEASUREMENT EQUATIONS AND TDI

For this study, we only include noises which are relevant to the performance of the clock noise reduction algorithm. These are readout noises N_i^s , N_i^{sb} , N_i^ϵ , N_i^τ , and $N_i^{\text{sb},\tau}$, sideband modulation errors M_i , and clock noise q_i . Clock noise is defined in terms of fractional frequency deviations, such that it couples into the measurements scaled by the absolute value of the beatnote frequency. M_i is defined in terms of fractional frequency deviations relative to the modulation frequency.

We assume that a pilot tone is used as phase reference on board each spacecraft [17]. In particular, this pilot tone is used to remove any additional clock jitters due to the Analog-Digital Converters (ADC). As such, q_i are the fractional frequency deviations of that pilot tone. M_i are additional deviations present in the sidebands relative to that same pilot tone, *e.g.*, due to noise added by the electro-optical modulators or the fibre amplifiers. Any residual clock jitter due to imperfections in the pilot tone correction is absorbed into the readout noise terms.

All noise signals depend on time, but this time dependency is not stated explicitly in this article, for readability's sake.

A. Interferometric measurements

For all interferometric measurements, we model only frequency deviation from a constant beatnote frequency, in units of Hz.

The science interferometric measurements s_1 and $s_{1'}$ are defined in terms of the beatnotes between the distant and local beams, on spacecraft i .

$$s_1 = \mathcal{F}[-a_1 \theta_1^s q_1 + N_1^s], \quad (7)$$

$$s_{1'} = \mathcal{F}[-a_{1'} \theta_{1'}^s q_1 + N_{1'}^s]. \quad (8)$$

The test-mass measurements ϵ_i and $\epsilon_{i'}$ are the beatnotes between the adjacent beam after it has bounced onto the local test-mass, and the

local beam, on spacecraft i . They read

$$\epsilon_1 = \mathcal{F}[-b_1 \theta_1^\tau q_1 + N_1^\epsilon], \quad (9)$$

$$\epsilon_{1'} = \mathcal{F}[-b_{1'} \theta_{1'}^\tau q_1 + N_{1'}^\epsilon]. \quad (10)$$

Similarly, the reference measurements τ_i and $\tau_{i'}$ are formed by the beatnote between the adjacent and local beams, without any bouncing on the test-mass. They read

$$\tau_1 = \mathcal{F}[-b_1 \theta_1^\tau q_1 + N_1^\tau], \quad (11)$$

$$\tau_{1'} = \mathcal{F}[-b_{1'} \theta_{1'}^\tau q_1 + N_{1'}^\tau]. \quad (12)$$

In addition to the carrier-carrier measurements, we also model sideband-sideband beatnotes. These are similar to the carrier-carrier beatnotes but contain additional clock noise terms which are amplified by a factor of $\frac{\nu_i^\tau}{a_i} \approx 100$ as well as more readout noise.

The sideband measurements in the science interferometers are defined as the beatnote between the distant and local upper sidebands. Their expressions read

$$\begin{aligned} s_1^{\text{sb}} = \mathcal{F} & \left[\theta_1^s (\nu_{2'}^m \mathcal{D}_3 (q_2 + M_{2'}) \right. \\ & \left. - \nu_1^m (q_1 + M_1) \right. \\ & \left. - (a_1 + \nu_{2'}^m - \nu_1^m) q_1 \right) + N_1^{\text{sb}} \right], \end{aligned} \quad (13)$$

$$\begin{aligned} s_{1'}^{\text{sb}} = \mathcal{F} & \left[\theta_{1'}^s (\nu_3^m \mathcal{D}_{2'} (q_3 + M_3) \right. \\ & \left. - \nu_{1'}^m (q_1 + M_{1'}) \right. \\ & \left. - (a_{1'} + \nu_3^m - \nu_{1'}^m) q_1 \right) + N_{1'}^{\text{sb}} \right]. \end{aligned} \quad (14)$$

There is also a sideband beatnote present in each reference interferometer, between the sidebands of the adjacent optical benches,

$$\begin{aligned} \tau_1^{\text{sb}} = \mathcal{F} & \left[\theta_1^\tau (\nu_{1'}^m (q_1 + M_{1'}) \right. \\ & \left. - \nu_1^m (q_1 + M_1) \right. \\ & \left. - (b_1 + \nu_{1'}^m - \nu_1^m) q_1 \right) + N_1^{\text{sb},\tau} \right], \end{aligned} \quad (15)$$

$$\begin{aligned} \tau_{1'}^{\text{sb}} = \mathcal{F} & \left[\theta_{1'}^\tau (\nu_1^m (q_1 + M_1) \right. \\ & \left. - \nu_{1'}^m (q_1 + M_{1'}) \right. \\ & \left. - (b_{1'} + \nu_1^m - \nu_{1'}^m) q_1 \right) + N_{1'}^{\text{sb},\tau} \right]. \end{aligned} \quad (16)$$

B. TDI variables

TDI intermediary variables ξ and η are constructed to remove primed laser noise, and opti-

cal bench displacement noise (here set to zero), respectively. They read [4]

$$\xi_1 = s_1 + \theta_1^s \theta_1^\tau \frac{\epsilon_1 - \tau_1}{2} + \theta_1^s \theta_2^\tau \frac{\mathcal{D}_3(\epsilon_{2'} - \tau_{2'})}{2}, \quad (17)$$

$$\xi_{1'} = s_{1'} + \theta_{1'}^s \theta_{1'}^\tau \frac{\epsilon_{1'} - \tau_{1'}}{2} + \theta_{1'}^s \theta_3^\tau \frac{\mathcal{D}_{2'}(\epsilon_3 - \tau_3)}{2}. \quad (18)$$

and

$$\eta_1 = \theta_1^s \xi_1 + \frac{\mathcal{D}_3(\theta_2^\tau \tau_{2'} - \theta_2^\tau \tau_2)}{2}, \quad (19)$$

$$\eta_{1'} = \theta_{1'}^s \xi_{1'} - \frac{\theta_{1'}^\tau \tau_{1'} - \theta_1^\tau \tau_1}{2}. \quad (20)$$

Inserting eqs. (7) to (16) into these expressions

yields

$$\eta_1 = -b_{2'} \mathcal{D}_3 \mathcal{F} q_2 - a_1 \mathcal{F} q_1 + \theta_1^s \mathcal{F} N_1^s + \theta_{1'}^\tau \frac{\mathcal{F}(N_1^\tau - N_1^\epsilon)}{2} + \theta_{2'}^\tau \frac{\mathcal{D}_3 \mathcal{F}(N_2^\tau + N_{2'}^\epsilon)}{2}, \quad (21)$$

$$\eta_{1'} = (b_{1'} - a_{1'}) \mathcal{F} q_1 + \theta_{1'}^s \mathcal{F} N_{1'}^s - \theta_{1'}^\tau \mathcal{F} N_{1'}^\tau - \theta_{1'}^\tau \frac{\mathcal{F}(N_1^\tau - N_{1'}^\epsilon)}{2} + \theta_3^\tau \frac{\mathcal{D}_{2'} \mathcal{F}(N_3^\tau - N_3^\epsilon)}{2}. \quad (22)$$

From these intermediary variables, we can build laser noise-free TDI variables. They can be expressed as polynomials of delay operators P_i and $P_{i'}$, in the form

$$\text{TDI} = \sum_{i=1,2,3} (P_i \eta_i + P_{i'} \eta_{i'}). \quad (23)$$

In appendix B, we give the expressions for the most common TDI variables. In the following, we will focus on first and second-generation Michelson variables X_1 and X_2 (and their circular permutations Y and Z), and first and second-generation Sagnac variables α_1 and α_2 (and their circular permutations β and γ).

C. Clock noise residuals

Inserting eqs. (21) and (22) into eq. (23), and keeping only clock noise, we observe that the clock residual in the variable reads

$$\text{TDI}^q = - \sum_{i=1}^3 (a_i P_i + a_{i'} P_{i'}) + b_{i'} [P_{i'} - P_{i-1} \mathcal{D}_{i+1}] q_i. \quad (24)$$

In this section, we assume that all armlengths are equal and constant². Also, we suppose that all clock noises are uncorrelated but have the same PSD $S_q(\omega)$. Under these assumptions, the clock noise residuals PSD is given by

² Therefore, we can commute delay operators with each

$$S_{\text{TDI}^q}(\omega) \approx S_q(\omega) \sum_{i=1}^3 \left| a_i \tilde{P}_i(\omega) + a_{i'} \tilde{P}_{i'}(\omega) + b_{i'} [\tilde{P}_{i'}(\omega) - \tilde{P}_{i-1}(\omega) \tilde{D}_{i+1}(\omega)] \right|^2. \quad (25)$$

Here, \tilde{D}_i is the Fourier transform of a delay operator, see [13] for further information. In the following paragraphs, we apply this formula to give an estimate of the clock noise residuals in the case of the Michelson and Sagnac variables.

1. Michelson variables

Using eq. (25), we can work out the clock noise residuals in the Michelson variables defined in appendix B. Before clock noise reduction, their PSD read

$$\begin{aligned} S_{X_1^q}(\omega) &\approx 4 \sin^2(\omega L) \left| \tilde{f}(\omega) \right|^2 S_q(\omega) \\ &\times \left[(a_1 - a_{1'})^2 + a_{2'}^2 + a_3^2 \right. \\ &\quad \left. + 4b_{1'}(a_1 - a_{1'} + b_{1'}) \sin^2(\omega L) \right]. \end{aligned} \quad (26)$$

Here, $\tilde{f}(\omega)$ is the transfer function of the anti-aliasing filter.

Because we assume that armlengths are constant, the delays commute and the second-

generation Michelson combination X_2 has a very simple relationship to the first-generation combination X_1 ³,

$$X_2 \approx (\mathcal{D}_{2'233'} - I)X_1. \quad (27)$$

We can use this relationship to estimate the residual clock noise in X_2 :

$$S_{X_2^q}(\omega) \approx 4 \sin^2(2\omega L) S_{X_1^q}(\omega). \quad (28)$$

Observe that this is only valid if the noise in question is not suppressed by TDI, such that additional terms due to delay commutators can be neglected. This approximation does not hold for laser noise, for example, as shown in [13].

2. Sagnac variables

Following the same technique and using the same assumptions, we can work out the residual clock noise in the both generations of the Sagnac variables,

$$\begin{aligned} S_{\alpha_1^q}(\omega) &= [(a_1 + b_{1'})^2 + (a_2 + b_{2'})^2 + (a_3 + b_{3'})^2 \\ &\quad + (a_{1'} - b_{1'})^2 + (a_{2'} - b_{2'})^2 + (a_{3'} - b_{3'})^2 - 2a_1 a_{1'} \\ &\quad - 2((a_{2'} - b_{2'})(a_2 + b_{2'}) + (a_{3'} - b_{3'})(a_3 + b_{3'})) \cos(\omega L) \\ &\quad + 2b_{1'}(a_1 - a_{1'} + b_{1'}) \cos(3\omega L)] \left| \tilde{f}(\omega) \right|^2 S_q(\omega), \end{aligned} \quad (29)$$

other, as well as delay and filter operators. As shown in [13], these commutators only yield multiplicative terms $\ll 1$.

³ In the limit of very low frequency, X_2 is thus similar to the time derivative of X_1 .

Again, there exists a simple relationship between the first and second-generation clock noise residuals for the Sagnac variables,

$$S_{\alpha_2^q}(\omega) = 4 \sin^2\left(\frac{3\omega L}{2}\right) S_{\alpha_1^q}(\omega) \quad (30)$$

IV. CLOCK NOISE REDUCTION

A. Sideband measurements

The sideband measurements are used to construct an independent measurement r_i of the differential clock noise between two spacecraft,

$$r_1 = \theta_1^s \frac{s_1 - s_1^{\text{sb}}}{\nu_{2'}^m}, \quad (31)$$

$$r_{1'} = \theta_{1'}^s \frac{s_{1'} - s_{1'}^{\text{sb}}}{\nu_3^m}. \quad (32)$$

Since the interferometric measurements are defined in units of Hz, r_i is dimensionless.

By inserting eqs. (7) and (8) and eqs. (13) and (14) into these expressions, we get

$$\begin{aligned} r_1 = & \mathcal{F} \left(q_1 + \frac{\nu_1^m}{\nu_{2'}^m} M_1 \right) \\ & - \mathcal{F} \mathcal{D}_3 (q_2 + M_{2'}) \\ & + \frac{\theta_1^s}{\nu_{2'}^m} \mathcal{F} (N_1^s - N_1^{\text{sb}}), \end{aligned} \quad (33)$$

$$\begin{aligned} r_{1'} = & \mathcal{F} \left(q_1 + \frac{\nu_{1'}^m}{\nu_3^m} M_{1'} \right) \\ & - \mathcal{F} \mathcal{D}_{2'} (q_3 + M_3) \\ & + \frac{\theta_{1'}^s}{\nu_3^m} \mathcal{F} (N_{1'}^s - N_{1'}^{\text{sb}}). \end{aligned} \quad (34)$$

If we again neglect everything but clock noise, we see that

$$r_1 \approx \mathcal{F} q_1 - \mathcal{F} \mathcal{D}_3 q_2, \quad (35)$$

$$r_{1'} \approx \mathcal{F} q_1 - \mathcal{F} \mathcal{D}_{2'} q_3. \quad (36)$$

Thus, the r_i measure the differential fractional frequency deviations of the different spacecraft clocks.

These terms will be used in section IVD to construct clock-noise reducing expressions.

B. Removal of primed modulation noise

In LISA, the Electro-Optical Modulators (EOM) on the primed optical benches will be running at different frequencies. For this document, we assume the preliminary values of 2.401 GHz for the primed and 2.4 GHz for the unprimed optical benches. The frequency distribution system ensures that the pilot tone used as phase reference for all phase measurements and the 2.4 GHz signal have a very stable phase relationship. The 2.401 GHz signal, on the other hand, is generated independently and thus contains additional noise compared to the pilot tone.

In our model, this corresponds to a higher value of the $M_{i'}$ compared to the M_i . We can remove the primed optical noises by using the sideband-sideband beatnote in the reference interferometers⁴. Let us define

$$\Delta M_1 = \theta_{1'}^s \left[\frac{\tau_1^{\text{sb}} - \tau_1}{2} + \frac{\tau_{1'}^{\text{sb}} - \tau_{1'}}{2} \right]. \quad (37)$$

These expressions are free of laser noise. Keeping only modulation error terms, we have

$$\Delta M_1 \approx \mathcal{F} (\nu_1^m M_1 - \nu_{1'}^m M_{1'}). \quad (38)$$

We can remove the primed optical bench EOM noise at the expense of adding more readout noise to the r_i variables,

$$r_1^c = r_1 - \frac{\mathcal{D}_3 \Delta M_2}{\nu_{2'}^m}, \quad (39)$$

$$r_{1'}^c = r_{1'} + \frac{\Delta M_1}{\nu_3^m}. \quad (40)$$

If we assume that the modulation frequencies are almost identical on all optical benches $\nu_i^m = \nu_{i'}^m = \nu^m$, we can estimate the residual noise in the r_i^c variables,

⁴ Another option would be to use an electronic beatnote

between the two modulation signals.

$$r_1^c \approx \mathcal{F}(M_1 + q_1) + \mathcal{D}_3 \mathcal{F}(M_{2'} - M_2) - \mathcal{F} \mathcal{D}_3(M_{2'} + q_2) + \theta_1^s \frac{\mathcal{F}(N_1^s - N_1^{\text{sb}})}{\nu^m} + \theta_{2'}^\tau \frac{\mathcal{D}_3 \mathcal{F}(N_2^\tau - N_2^{\text{sb},\tau} + N_{2'}^\tau - N_{2'}^{\text{sb},\tau})}{2\nu^m}, \quad (41)$$

$$r_{1'}^c \approx \mathcal{F}(M_1 + q_1) - \mathcal{F} \mathcal{D}_{2'}(M_3 + q_3) + \theta_{1'}^s \frac{\mathcal{F}(N_{1'}^s - N_{1'}^{\text{sb}})}{\nu^m} - \theta_{1'}^\tau \frac{\mathcal{F}(N_1^\tau - N_1^{\text{sb},\tau} + N_{1'}^\tau - N_{1'}^{\text{sb},\tau})}{2\nu^m}. \quad (42)$$

Primed modulation terms do not show up in $r_{1'}^c$, but in r_1^c , $M_{2'}$ appears multiplied by a delay-filter commutator. These commutators have a magnitude proportional to the armlength rate of

change $\dot{L} \approx 1 \times 10^{-8}$ [13]. Neglecting them in the previous expression leads to an approximate calibrating variable, where the primed modulation term $M_{2'}$ has disappeared,

$$r_1^c \approx \mathcal{F}(M_1 + q_1) - \mathcal{D}_3 \mathcal{F}(M_2 + q_2) + \theta_1^s \frac{\mathcal{F}(N_1^s - n_1^{\text{sb}})}{\nu^m} + \theta_{2'}^\tau \frac{\mathcal{D}_3 \mathcal{F}(N_2^\tau - N_2^{\text{sb},\tau} + N_{2'}^\tau - N_{2'}^{\text{sb},\tau})}{2\nu^m} \quad (43)$$

C. Former clock-noise reduction algorithms

1. Michelson variables

A clock-noise reducing expression for the first-generation Michelson variable X_1 was proposed in [19], and reads

$$K_{X_1} = \frac{b_{1'}}{2} [(1 - \mathcal{D}_{33'})(r_{1'} + \mathcal{D}_{2'} r_3) + (1 - \mathcal{D}_{2'2})(r_1 + \mathcal{D}_3 r_{2'})] + a_1(r_{1'} + \mathcal{D}_{2'} r_3) - a_{1'}(r_1 + \mathcal{D}_3 r_{2'}) + a_{2'}[r_{1'} - (1 - \mathcal{D}_{2'2})r_1 + \mathcal{D}_{2'} r_3] - a_3[r_1 - (1 - \mathcal{D}_{33'})r_{1'} + \mathcal{D}_3 r_{2'}], \quad (44)$$

such that clock noise is strongly suppressed in $X_1^c = X_1 - K_{X_1}$. In [18], it was adapted for second generation under the assumption that delays commute, such that

$$X_2^c = X_2 - K_{X_2} = X_2 - (1 - \mathcal{D}_{33'2'2})K_{X_1}. \quad (45)$$

If we account for time-varying armlengths, these expressions have non-vanishing clock noise

residuals for both generations. For the first-generation X_1 , and ignoring the filters, these residuals read

$$X_1^{c,q} = \frac{b_{1'}}{2} [\mathcal{D}_{33'}, \mathcal{D}_{2'2}] q_1, \quad (46)$$

while those for the second generation are

$$\begin{aligned}
X_2^{c,q} = & b_{1'} \left(\frac{1}{2} [\mathcal{D}_{33'}, \mathcal{D}_{2'2}] (1 + \mathcal{D}_{33'2'2}) + \frac{1}{2} [\mathcal{D}_{33'2'2}, \mathcal{D}_{2'233'}] - [\mathcal{D}_{33'}, \mathcal{D}_{2'2}] \mathcal{D}_{33'} \right) q_1 \\
& + (a_{1'} [\mathcal{D}_{33'}, \mathcal{D}_{2'2}] \mathcal{D}_{33'} + a_1 [\mathcal{D}_{33'}, \mathcal{D}_{2'2}]) q_1 \\
& + a_{2'} [\mathcal{D}_{33'}, \mathcal{D}_{2'2}] \mathcal{D}_3 q_2 + a_3 [\mathcal{D}_{33'}, \mathcal{D}_{2'2}] \mathcal{D}_{33'2'} q_3.
\end{aligned} \tag{47}$$

From eqs. (46) and (47), following the procedure outline in [13], we compute the PSD of the residual clock noise in the corrected variables at leading order in the armlength derivatives:

$$S_{X_1^{c,q}}(\omega) \approx 4b_{1'}^2 \omega^2 L^2 (\dot{L}_2 - \dot{L}_3)^2 \left| \tilde{f}(\omega) \right|^2 S_q(\omega), \tag{48}$$

$$\begin{aligned}
S_{X_2^{c,q}}(\omega) \approx & 8\omega^2 L^2 (\dot{L}_2 - \dot{L}_3)^2 [b_{1'} (2a_1 + b_{1'}) \cos(4\omega L) \\
& + 2b_{1'} (a_1 - 2a_{1'}) + 2(a_1^2 + a_3^2 + a_{1'}^2 + a_{2'}^2) + 3b_{1'}^2 \\
& + 4(a_1 + b_{1'}) (a_{1'} - b_{1'}) \cos(2\omega L)] \left| \tilde{f}(\omega) \right|^2 S_q(\omega).
\end{aligned} \tag{49}$$

2. Sagnac variables

Similar to the Michelson variables, the clock-noise reducing expression for the first-generation Sagnac variable α_1 was first proposed in [19], and reads

$$\begin{aligned}
K_{\alpha_1} = & \frac{b_{1'}}{2} [(r_1 + \mathcal{D}_3 r_2 + \mathcal{D}_{31} r_3) + (r_{1'} + \mathcal{D}_{2'} r_{3'} + \mathcal{D}_{2'1'} r_{2'})] \\
& + (b_{2'} + a_2) r_1 + (b_{2'} - a_{2'}) (r_{1'} + \mathcal{D}_{2'} r_{3'}) \\
& + (b_{3'} - a_{3'}) r_{1'} + (b_{3'} + a_3) (r_1 + \mathcal{D}_3 r_2),
\end{aligned} \tag{50}$$

such that $\alpha_1^c = \alpha_1 - K_{\alpha_1}$ is almost free of clock noise. In [18], it was adapted for second generation, such that

$$\alpha_2^c = \alpha_2 - K_{\alpha_2} = \alpha_2 - (1 - \mathcal{D}_{312}) K_{\alpha_1}. \tag{51}$$

These corrected expressions also have non-vanishing clock noise residuals for both genera-

tions, if we account for time-varying armlengths. The residuals for the first-generation corrected α_1 are, if one neglects the filters,

$$\alpha_1^{c,q} = \frac{b_{1'}}{2} (\mathcal{D}_{312} - \mathcal{D}_{2'1'3'}) q_1, \tag{52}$$

whilst those for the second generation read

$$\begin{aligned}
\alpha_2^{c,q} = & \left(b_{1'} [\mathcal{D}_{2'1'3'}, \mathcal{D}_{312}] + (a_1 + \frac{b_{1'}}{2} (1 + \mathcal{D}_{312})) (\mathcal{D}_{2'1'3'} - \mathcal{D}_{312}) \right) q_1 \\
& + (a_2 + b_{2'}) (\mathcal{D}_{2'1'3'} - \mathcal{D}_{312}) \mathcal{D}_3 q_2 + (a_3 + b_{3'}) (\mathcal{D}_{2'1'3'} - \mathcal{D}_{312}) \mathcal{D}_{31} q_3.
\end{aligned} \tag{53}$$

Here, we used that

$$\begin{aligned}
a_1 + a_2 + a_3 - a_{1'} - a_{2'} - a_{3'} \\
+ 2b_{1'} + 2b_{2'} + 2b_{3'} \approx 0,
\end{aligned} \tag{54}$$

which is exact when Doppler shifts are neglected, but remains a good approximation even when

Doppler shifts are included in the beatnote definition [18].

These residuals do not only involve a commutator but also a plain difference between different armlengths. Therefore, leading order in the arm-

length derivatives is the zeroth order. At this order, the corresponding PSDs for the residual clock jitter in the corrected Sagnac variables read

$$S_{\alpha_1^{c,q}}(\omega) \approx b_1^2 \sin^2\left(\omega \frac{\sigma_L - \sigma_{L'}}{2}\right) \left| \tilde{f}(\omega) \right|^2 S_q(\omega), \quad (55)$$

$$S_{\alpha_2^{c,q}}(\omega) \approx 4 \sin^2\left(\omega \frac{\sigma_L - \sigma_{L'}}{2}\right) \left[-b_{1'}(2a_1 + b_{1'}) \sin^2\left(\omega \frac{\sigma_L}{2}\right) + (a_1 + b_{1'})^2 + (a_2 + b_{2'})^2 + (a_3 + b_{3'})^2 \right] \left| \tilde{f}(\omega) \right|^2 S_q(\omega), \quad (56)$$

where we have defined $\sigma_L = L_1 + L_2 + L_3$ and $\sigma_{L'} = L_{1'} + L_{2'} + L_{3'}$.

D. Exact algorithms for clock-noise reduction

1. Principle of exact clock-noise reduction

We recognize that the clock noise terms enter eqs. (35) and (36) with the same structure as laser noise in the η_i variables. They indeed represent the six one-way interferometric measurements, each containing one local clock noise and one remote clock noise delayed by the corresponding armlength. From these building blocks, we can apply the reasoning outlined in [20] to synthesize arbitrary virtual photon paths of the form

$$q_B - \mathcal{D}_{i_n i_{n-1} \dots i_1} q_A, \quad (57)$$

where the indices $i_1 \dots i_n$ correspond to a valid path connecting spacecraft A to B . Following our indexing convention in fig. 1, this means formally that

- The spacecraft pointed to by the link i_k should be the starting point of link i_{k+1} , for any $k < n$.

- The first link i_1 should start from spacecraft A .
- The last link i_n should point to spacecraft B .

By combining multiple such expressions, we can construct polynomials of delay operators of the form

$$\sum_i P_i q_i, \quad (58)$$

where the delays in the polynomials P_i pairwise correspond to photon paths.

If the polynomials $P_i, P_{i'}$ in eq. (24) are also of this form, we can construct six expressions $R_i, R_{i'}$ out of the $r_i, r_{i'}$ variables such that

$$R_i = P_i q_i \quad \text{and} \quad R_{i'} = P_{i'} q_{i'}. \quad (59)$$

Thus, we find a general expression for any TDI variable satisfying the above condition⁵

$$\text{TDI}^c = \text{TDI} - \left(\sum_{i=1}^3 b_{(i+1)'} P_i r_i^c - (a_i + b_{(i+1)'}) R_i - (a_{i'} - b_{i'}) R_{i'} \right). \quad (60)$$

⁵ Here, we used that $P_{i-1} \mathcal{D}_{i+1} q_i = R_{i-1} - P_{i-1} r_{i-1}^c$. This is an immediate consequence of eqs. (35) and (59).

In the following, we use this principle to find clock noise-free expressions for both first and second-generation Michelson variables, as well as the second-generation Sagnac variables. As a counterexample, the first-generation Sagnac variable can't be factored as described above, and thus exact clock noise removal by this method is impossible. See appendix C for an overview over some of the most commonly used TDI variables.

Note that these corrections are only exact under the strong assumption that there are no Doppler effects and the beatnote frequencies

remain constants. In the following sections, we exclusively work under this assumption.

2. Michelson variables

We recognize that the delay polynomials for the Michelson variables in eqs. (B1) and (B2) correspond to photon paths. As such, we can derive the following clock-noise reducing expressions,

$$K_{X_1} = a_3(1 - \mathcal{D}_{33'})r_{1'}^c - a_{2'}(1 - \mathcal{D}_{2'2})r_1^c - (a_{1'} + a_3)(r_1^c + \mathcal{D}_3r_{2'}^c) + (a_1 + a_{2'} + b_{1'}(1 - \mathcal{D}_{33'}))(r_{1'}^c + \mathcal{D}_{2'}r_3^c), \quad (61)$$

$$K_{X_2} = a_3(1 - \mathcal{D}_{33'} - \mathcal{D}_{33'2'2} + \mathcal{D}_{2'233'33'})r_{1'}^c - a_{2'}(1 - \mathcal{D}_{2'2} - \mathcal{D}_{2'233'} + \mathcal{D}_{33'2'22'2})r_1^c - (a_{2'} + a_1 + a_{1'} + a_3)(1 - \mathcal{D}_{2'2})(r_1^c + \mathcal{D}_3r_{2'}^c) + (a_1 + a_{2'} + a_{1'} + a_3)(1 - \mathcal{D}_{33'})(r_{1'}^c + \mathcal{D}_{2'}r_3^c) - (a_{1'} + a_3)(1 - \mathcal{D}_{2'233'})(r_1^c + \mathcal{D}_3r_{2'}^c) + (a_1 + a_{2'})(1 - \mathcal{D}_{33'2'2})(r_{1'}^c + \mathcal{D}_{2'}r_3^c) + b_{1'}(1 - \mathcal{D}_{33'} - \mathcal{D}_{33'2'2} + \mathcal{D}_{2'233'33'})(r_{1'}^c + \mathcal{D}_{2'}r_3^c). \quad (62)$$

Compared to the method described in [18], the expressions that we propose exactly cancel clock noise, even if we account for time-varying armlengths. Besides, they have a reduced number of correction terms. In section V, we study the secondary noises which enter the corrected expressions and limit the performance of the new algorithm.

3. Sagnac Variables

In [18], it is claimed that an exact cancellation of clock noise is impossible for second-generation Sagnac variables. The argument is

that second-generation Sagnac variables can be related to their first-generation counterparts under the assumptions that delays commute, and that Sagnac effect can be neglected for clock noise. Because an exact cancellation of clock noise for first-generation Sagnac variables [19], it was thought that such a method is also impossible for the second generation. In this section, we show that an exact clock-jitter reduction for second-generation Sagnac variables is possible and we propose an algorithm.

If we factor the Sagnac variable according to eq. (23), we recognize that the delay polynomials correspond to valid photon paths. Thus, we can derive the exact clock-noise reducing expression

$$K_{\alpha_2} = a_1(1 - \mathcal{D}_{2'1'3'})r_1^c - (a_{1'} - b_{1'})(1 - \mathcal{D}_{312})r_{1'}^c + (a_3 + b_{1'} + b_{3'})(1 - \mathcal{D}_{2'1'3'})\mathcal{D}_3r_2^c + (a_{2'} - b_{2'})(1 - \mathcal{D}_{312})\mathcal{D}_{2'}r_3^c - b_{1'}(1 - \mathcal{D}_{2'1'3'})\mathcal{D}_{31}r_{3'}^c, \quad (63)$$

such that the corrected Sagnac variable $\alpha_2^c = \alpha_2 - K_{\alpha_2}$ is free of clock noise.

V. RESIDUAL NOISES IN THE CORRECTED VARIABLES

A. Flexing-filtering coupling

When deriving the clock-noise suppressing terms in the previous sections, we have neglected the filter operators in the r_i and $r_{i'}$ variables. Accounting for the filters, the algorithm is no longer exact as delay-filter commutators appear. As shown in [13], these delay-filter commutators contribute to the flexing-filtering coupling in the Michelson variables presented in eqs. (61) and (62), and the second-generation Sagnac variable in eq. (63). The time-domain expressions are given in appendix D.

Following the methods used in [13] to estimate the flexing-filtering for the residual laser noise in

the Michelson variables, we find that the flexing-filtering coupling associated with clock noise reads, to first order in powers of the armlength derivatives,

$$S_{X_1^{c,\mathcal{F}}}(\omega) \approx 4\omega^2((A_1^2 + b_{1'}^2)\dot{L}_2^2 + a_1^2\dot{L}_3^2) \times \sin^2(\omega L)K_f(\omega)S_q(\omega), \quad (64)$$

$$S_{X_2^{c,\mathcal{F}}}(\omega) \approx 4\sin^2(2\omega L)S_{X_1^{c,\mathcal{F}}}(\omega), \quad (65)$$

where we have defined $A_1 = a_{1'} - b_{1'}$. $K_f(\omega) = \left| \frac{d\tilde{f}(\omega)}{d\omega} \right|^2$ is the squared modulus of the filter transfer function derivative⁶. We neglected Doppler shifts to obtain these compact expressions. However, they give a relatively good estimate up to around 10% of the residual flexing-filtering coupling in the LISA frequency range.

We use the same procedure to estimate the flexing-filtering coupling associated with clock noise in the Sagnac variable, to first order in powers of the armlength derivatives. We find

$$S_{\alpha_2^{c,\mathcal{F}}} \approx 4\omega^2 \sin^2\left(\frac{3\omega L}{2}\right) [(A_2^2 + A_3^2)\dot{L}_1^2 + (A_1^2 + b_{1'}^2)\dot{L}_2^2 + a_1^2\dot{L}_3^2 + 2\dot{L}_1(A_1A_3\dot{L}_2 + a_1A_2\dot{L}_3) \cos \omega L] K_f(\omega)S_q(\omega), \quad (66)$$

where we have defined $A_1 = a_{1'} - b_{1'}$, $A_2 = a_{1'} - b_{2'}$, and $A_3 = a_3 + b_{1'} + b_{3'}$.

B. Readout noise

The readout noise entering the r_i^c variables appears scaled by the inverse of the modulation

frequency $\nu_m \approx 2.4$ GHz in eqs. (41) and (42). These r_i^c variables are scaled in the corrected Michelson combinations (eqs. (61) and (62)) by the beatnote frequencies a_i and b_i , which are always smaller than 25 MHz. As such, the additional readout noise introduced by our clock-noise reduction algorithm is suppressed by the factors a_i/ν^m and b_i/ν^m of the order 10^{-2} , and therefore below the readout noise already present in the data. This is why we neglect the additional readout noise in the residual clock noise, *c.f.* section VII.

⁶ The dominant contribution to the K_f term is the group delay of the filter. As shown in [13], compensating for the filter group delay significantly decreases contributions from this term but does not fully remove them.

C. Modulation errors

To estimate modulation errors, we assume in this section that the modulation frequencies are equal, so we can use eqs. (41) and (42). In addition, we neglect flexing-filtering coupling for the modulation noise, as well as the additional readout noise in these expressions.

The remaining modulation error terms M_i enter eqs. (41) and (42) with the same pattern as clock noise. Since the new algorithm perfectly removes clock noise from the TDI variables, modulation errors in the corrected variables are identical to the clock-noise terms in the uncorrected variables. As such, following eqs. (26) and (28), their PSDs are given by

$$S_{X_1^M}(\omega) \approx 4 \sin^2(\omega L) \left| \tilde{f}(\omega) \right|^2 S_M(\omega) \times \left[(a_1 - a_{1'})^2 + a_{2'}^2 + a_3^2 + 4b_{1'}(a_1 - a_{1'} + b_{1'}) \sin^2(\omega L) \right], \quad (67)$$

$$S_{X_2^M}(\omega) \approx 4 \sin^2(2\omega L) S_{X_1^M}(\omega), \quad (68)$$

where we again assume that modulation noise is uncorrelated but of equal PSD $S_M(\omega)$ for all 2.4 GHz sidebands.

VI. SIMULATION

We present here the simulations that are used to generate realistic LISA measurements, compute the TDI combinations from these measurements, and apply the algorithm proposed in the previous section to reduce clock noise. Details about the `LISANode` simulator and the instrumental model are given below. Results are presented and discussed in section VII.

A. LISANode

`LISANode` is the baseline prototype for an end-to-end mission performance simulator. It is a

flexible tool that performs computations in the time domain to produce time series of realistic measurements that one expects from LISA, along with uncorrected and corrected TDI Michelson and Sagnac variables.

It is based on high-level simulation graphs defined in Python scripts. These graphs are composed of atomic computation units chained together, called nodes and written in C++ for computational efficiency. A scheduler triggers the node execution in a specific order and pushes data from one node to the next. In this manner, the execution time is optimized and data flow is synchronized.

All interferometric signals are represented as relative frequency deviations, or Doppler variables $\delta\nu/\nu_0$, where ν_0 is the laser frequency. They are implemented as doubles (64-bit floating-point numbers).

Two different sampling frequencies are used in our simulations. The *physical* sampling frequency is used to simulate all physical processes, such as generation of instrumental noise, propagation of laser beams, and optical measurements. It is here set to $f_{\text{phy}} = 30$ Hz. The measurement signals are s_i , s_i^{sb} , ϵ_i and τ_i are downsampled to the *measurement* frequency $f_{\text{meas}} = 3$ Hz by means of a decimation of a factor $f_{\text{phy}}/f_{\text{meas}} = 10$. All processing steps, including TDI and clock-noise reduction, are therefore carried out at this measurement frequency.

B. Instrumental modelling

The three spacecraft of the LISA constellation are simulated. Signals imprinted on laser beams are exchanged between the spacecraft. We use time-varying delays to model the propagation of these signals, implemented as Lagrange interpolating polynomials of order 31. They allow both for good precision and limited execution time and numerical errors.

The Keplerian orbits presented in [21] are used in this study. We then deduce the light travel times along each arm from the relative positions and velocities of the spacecraft [22].

These light travel times include contributions from the Sagnac effect, related to the rotation of the constellation, as well as first-order relativistic corrections.

Each spacecraft contains two optical benches, a clock, a phasemeter and an on-board computer. Each optical bench implements the latest *split interferometry* optical setup described in section IV and fig. 2: four interferometric measurements s_i , s_i^{sb} , ϵ_i and τ_i (respectively the science, sideband, test-mass and reference signals) are formed.

Relevant sources of noise are added to the measurements. We assume that the overwhelming laser frequency noise is a white noise at

$$\sqrt{S_p(f)} = 10^{-13} \text{ Hz}^{-1/2}. \quad (69)$$

Secondary noises, such as test-mass acceleration (TM) noise, optical path (OP) noise or read-out noise (RO) are used as a benchmark since they are not suppressed by TDI, but only have their spectra modulated. The spectral shapes of these sources of noise are given in [14], and read

$$\begin{aligned} \sqrt{S_{\text{TM}}(f)} &= 2.4 \times 10^{-15} \text{ ms}^{-2} \text{ Hz}^{-1/2} \\ &\times \left[1 + \left(\frac{4 \times 10^{-4} \text{ Hz}}{f} \right)^2 \right]^{1/2}, \end{aligned} \quad (70)$$

$$\sqrt{S_{\text{RO}} + S_{\text{OP}}(f)} \approx 10^{-11} \text{ m} \cdot \text{ Hz}^{-1/2}. \quad (71)$$

We assume that 15% of the light power is used for the sidebands, such that the shot noise level in them increases by a factor of $\sqrt{0.85/0.15}$.

For the modulation errors we use a simple model based on the fiber amplifier noise and their level as given in [17]

$$\begin{aligned} \sqrt{S_M(f)} &= 10^{-14} \text{ sHz}^{-1/2} \\ &\times \sqrt{1 + \left(\frac{1.5 \times 10^{-2} \text{ Hz}}{f} \right)^2}. \end{aligned} \quad (72)$$

They are added to the sidebands alongside the USO noise.

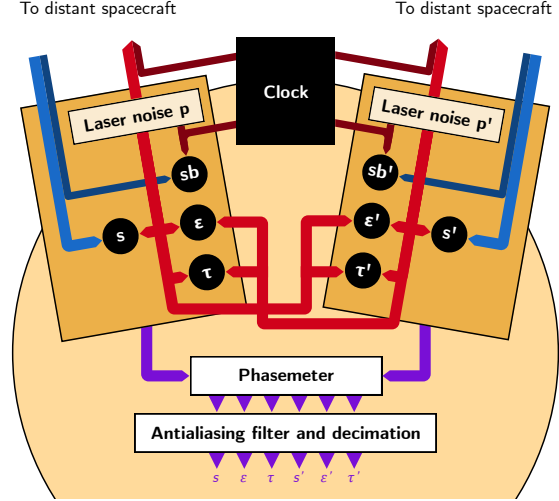


Figure 2. Optical design used in LISANode simulations. Eight interferometric measurements are performed for each spacecraft: two science signals s_i and $s_{i'}$, two side-band signals s_i^{sb} and $s_{i'}^{\text{sb}}$, two test-mass signals ϵ_i and $\epsilon_{i'}$, along with two reference signals, τ_i and $\tau_{i'}$.

These interferometric measurements are then transmitted to the phasemeter, where clock noise is added in the form of the USO noise, scaled by the beatnote frequency. We model the fractional frequency deviation of each USO by a flicker noise with a power spectrum of $S_q(f) = 6.7 \times 10^{-27}/f$, generated using a variant of the infinite RC model [23]. We add to this flicker noise a linear frequency deviation to account for the clock frequency drift.

The signals are then fed to the on-board computer, which decimates all signals down to 3 Hz. To prevent power folding, we use a symmetric Finite Impulse Response (FIR) anti-aliasing filter of order 253, implemented using a direct form I. Its coefficients are computed such that the signal is attenuated by 240 dB between 0.2 Hz and 0.9 Hz. The results of these operations are the measurement signals that one can expect from LISA.

C. Processing and clock-noise reduction

These measurements are used to form TDI intermediary variables and then Michelson variables X , Y and Z . The clock noise calibration algorithm presented in section IV is used to reduce the clock noise in the TDI channels. We finally obtain the clock-calibrated Michelson variables X^c , Y^c , and Z^c .

Similarly to what is done to model the propagation of signals between two spacecraft, pre-processing delays are implemented using Lagrange interpolating polynomials of order 31. To form Michelson variables, one must apply multiple delays to the interference measurements for the calculation of the Michelson variables X , Y , and Z . In order to minimize the error introduced by these interpolations, we use a nested delay algorithm in which a single interpolation is necessary.

VII. RESULTS AND DISCUSSION

In figs. 3 and 4, we present the results of the 2×10^6 s-long simulations described in the previous section, respectively for second-generation Michelson X_2 and Sagnac α_2 combinations. We use Welch's method to estimate the spectra, with segments of 80 000 samples and a *Nuttall4* window function. The following set of beatnote frequencies are used in the simulations and analytic models: $a_1 = a_2 = a_3 = -10$ MHz, $a_{1'} = a_{2'} = a_{3'} = 10$ MHz, $b_{1'} = b_{2'} = b_{3'} = 10$ MHz. Contrary to the analytic development presented in the previous sections, the following figures show fractional frequency deviations, *i.e.* the frequency deviation to the central laser frequency $\nu_0 \approx 2.8 \times 10^{14}$ MHz, normalized by the same frequency ν_0 .

We show that these simulations are in perfect agreement with the models presented in sections III and V for the residual clock noise before and after the correction.

In each of these figures, the blue and red solid curves show the residual clock noise in, respectively, the uncorrected and corrected TDI combination. Associated analytical models for the

residual clock noise are plotted as black dashed curves. They agree perfectly with the simulation results in a large fraction of the frequency band. Near the Nyquist frequency, we see an increase of the residual clock noise level in our simulated data. This increase is caused by errors in the Lagrange interpolation routine used to implement offline time delays, which we did not include in our analytical modelling. Indeed, increasing the interpolation order pushes this peak towards higher frequencies. Below 10^{-3} Hz, we see a noise floor in the simulated data that is not present in the analytical model. This is likely linked to limited numerical accuracy in our simulation. In addition, our assumption of linear armlengths is only valid at timescales up to one day, which could also explain this deviation.

The limiting modulation noise is presented as a magenta trace. We can see that is below the required level, which is here associated to the level of secondary noises in the uncorrected and corrected combination and represented by the light and dark teal solid curves. This is because TDI does not suppress these secondary noises, but only modulates their spectral shapes. Notice that both curves are superimposed, which shows that the correction does not add visible levels of extra readout noise.

The light and dark orange solid curves respectively show the laser noise residuals in the uncorrected and corrected combinations. We check here that clock-noise reduction algorithms do not yield any increasing of the laser noise.

VIII. CONCLUSION

In this article, we revisit the problem of clock-noise correction in space-based gravitational wave detectors. We find a general expression for the residual clock noise in any TDI variable, and provide a generic algorithm to derive clock-noise reducing expressions applicable to most TDI variables used in the literature.

We provide expressions for the residual clock noise levels after the correction, both for the new expressions derived in this article and for the previously published results for the Michelson

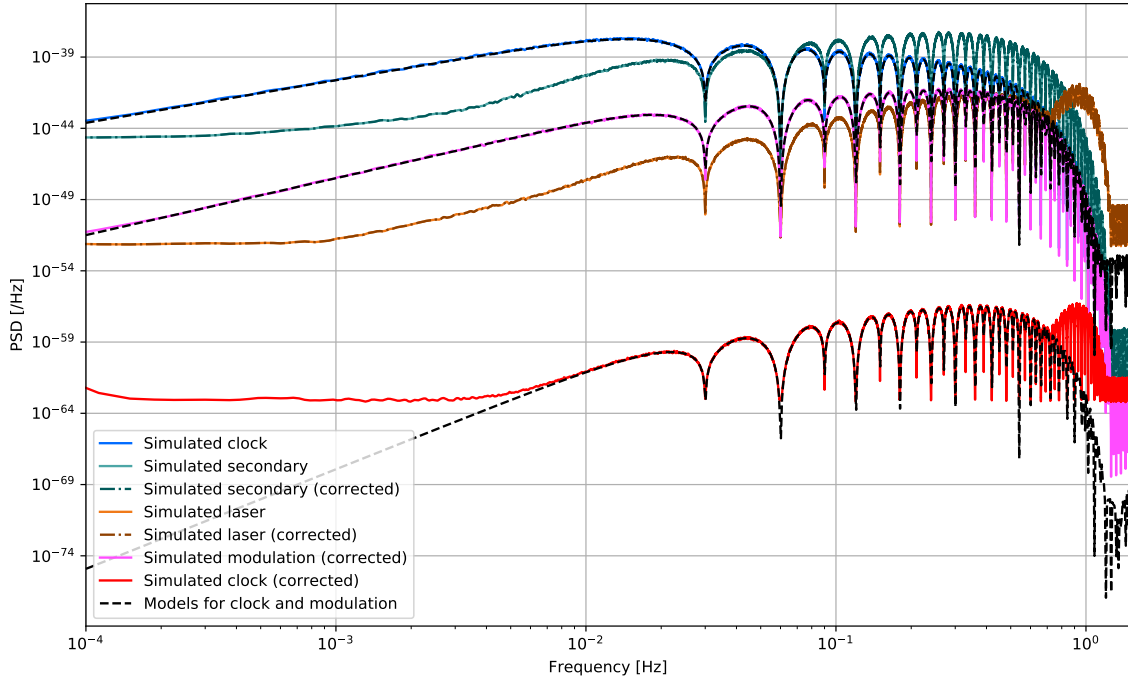


Figure 3. Power spectral density of the residual clock noise in the uncorrected X_2 and corrected X_2^c second-generation Michelson variables. We also plot the residual laser noise and the modulation errors. The secondary noises are given as a reference for the required noise levels and are close to an equivalent $10 \text{ pm}/\sqrt{\text{Hz}}$ at high frequencies.

and Sagnac variables [18]. We include the effect on-board antialiasing filters have on these residuals and provide estimates of their PSDs. The new expressions yield consistently lower residual noise levels than the previous results.

These analytical results are backed up by time-domain simulations using the simulator LISANode. In the simulation, the spacecraft positions are simulated according to Keplerian orbits and the signal delays are computed including relativistic corrections. In the analytical expressions, we assume that the armlengths can be described as linear functions of time. This assumption yields excellent agreement with our simulation results over a large frequency range.

In order to evaluate the clock noise suppression in comparison to other noise sources, we include simulations with only secondary noises and with only laser noise. We show that, us-

ing realistic values for the on-board USO, clock noise is dominating the overall noise level at low to mid frequencies if no clock-noise suppression is performed. With the suppression, the residual clock noise is far below both the level of secondary noises and the residual laser noise.

One of the limiting factors for clock noise correction is the phase fidelity between the pilot tone used as timing reference in the phasemeter and the clock sidebands used for the correction. We include a noise term describing errors in the modulation sidebands in our description, as well as an algorithm to remove half of these noise terms using sideband beatnotes in the reference interferometers. The remaining modulation noise exactly replaces the clock noise in the corrected TDI variable, thus imposing strict timing requirements on the signal chain from pilot tone to modulation sideband.

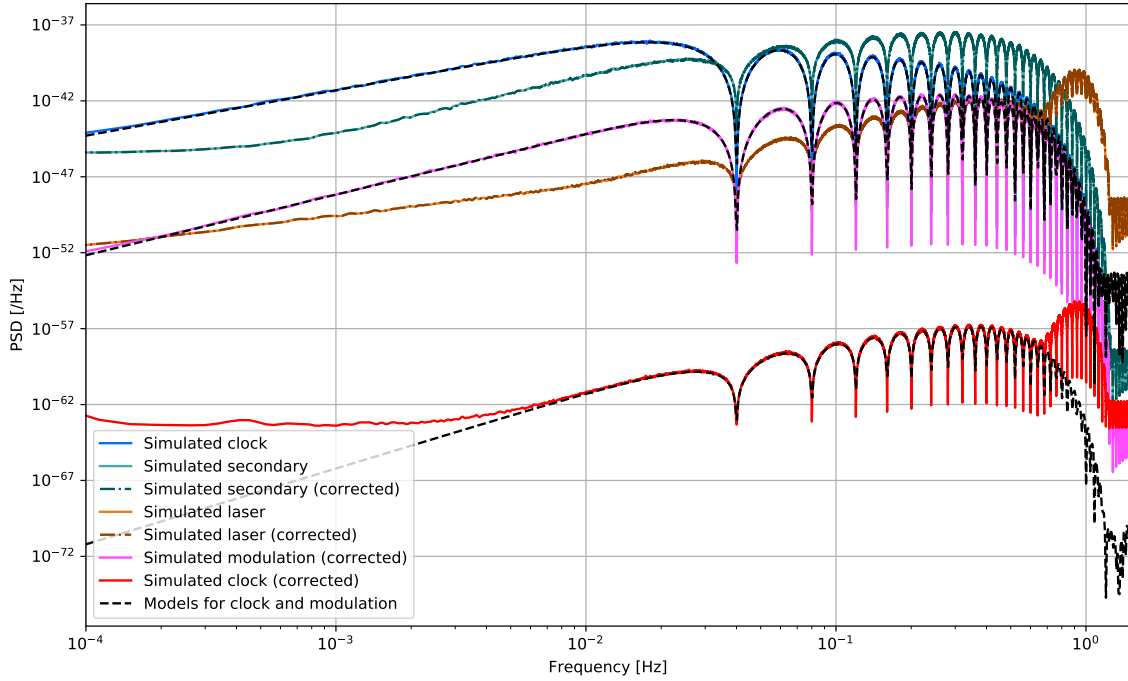


Figure 4. Power spectral density of the residual clock noise in the uncorrected α_2 and corrected α_2^c second-generation Sagnac variables. We also plot the residual laser noise and the modulation errors. The secondary noises are given as a reference for the required noise levels and are close to an equivalent $10 \text{ pm}/\sqrt{\text{Hz}}$ at high frequencies.

Future work on this topic could include a more realistic model for the beatnote frequencies, in particular accounting for the effect of Doppler shifts and laser locking. Other TDI specific

effects, such as coupling of errors in the absolute ranging or in the interpolation scheme, remain to be included in both our model and simulations as well.

Appendix A: Symbols

$\nu_i, \nu_{i'}$	Laser frequencies (Hz)
$\nu_i^m, \nu_{i'}^m$	Frequency offsets in the sidebands (Hz)
$a_i, a_{i'}$	Carrier beatnote frequencies in the science interferometers (Hz)
$b_i, b_{i'}$	Carrier beatnote frequencies in the test-mass and reference interferometers (Hz)
$c_i, c_{i'}$	Sideband beatnote frequencies in the science interferometers (Hz)
$\theta^s, \theta_{i'}^s, \theta^\tau, \theta_{i'}^\tau$	Science and reference beatnote polarities (dimensionless)
$L_i, L_{i'}, \mathcal{D}_i$	Light travel times (s) and associated delay operators
$f, \tilde{f}, \mathcal{F}$	Anti-aliasing filter kernel (s^{-1}), transfer function (dimensionless), and operator
$\tilde{x}(\omega)$	Fourier transform of a signal $x(t)$
$S_x(\omega)$	PSD of a signal $x(t)$
N_i^s, N_i^{sb}	Readout noises in the science and sideband interferometers (Hz)
N_i^e	Readout noises in the test-mass interferometers (Hz)
$N_i^\tau, N_i^{\text{sb}, \tau}$	Readout noises in the reference and sideband interferometers (Hz)
$M_i, S_M(\omega)$	Modulation errors (fractional frequency deviations, dimensionless), and PSD (Hz^{-1})
q_i, S_q	Clock noises (fractional frequency deviations, dimensionless), and associated PSD (Hz^{-1})
$\xi_i, \xi_{i'}, \eta_i, \eta_{i'}$	TDI intermediary variables (Hz)
$r_i, r_{i'}$	Clock-noise correction building blocks (fractional frequency deviations, dimensionless)
ΔM_i	Modulation-noise correcting intermediary variables (Hz)
$P_i, P_{i'}$	Polynomials of delay operators in a generalized TDI combination (dimensionless)
$R_i, R_{i'}$	Clock-noise correcting combinations of $r_i, r_{i'}$ (dimensionless)
X_1, X_2	Michelson first and second-generation variables (Hz)
α_1, α_2	Sagnac first and second-generation variables (Hz)
K_f	Squared modulus of frequency derivative of anti-aliasing filter transfer function (Hz^{-2})

Appendix B: TDI variable expressions

We give here the expressions of some laser noise-suppressing TDI variables in the form of Eq. 23. We only present one combination of each kind; the remaining ones can be deduced by circular permutation of indices. We always indicate the TDI generation using a lower index.

For the E_2 combination and some of the clock-noise correcting expressions in appendix C, we need not only delays, but also their inverse, or forward time shifts. These time advancements, which we denote by $\mathcal{D}_{\bar{k}}$, are defined by the property that $\mathcal{D}_{\bar{k}\bar{k}} = 1$.

1. Michelson variables

First-generation Michelson variable X_1 reads

$$X_1 = -(1 - \mathcal{D}_{2'2})\eta_1 + (1 - \mathcal{D}_{33'})\eta_{1'} - (1 - \mathcal{D}_{2'2})\mathcal{D}_3\eta_{2'} + (1 - \mathcal{D}_{33'})\mathcal{D}_{2'}\eta_3, \quad (\text{B1})$$

while second-generation X_2 is given by

$$X_2 = -(1 - \mathcal{D}_{2'2} - \mathcal{D}_{2'233'} + \mathcal{D}_{33'2'22'2})\eta_1 + (1 - \mathcal{D}_{33'} - \mathcal{D}_{33'2'2} + \mathcal{D}_{2'233'33'})\eta_{1'} \\ - (1 - \mathcal{D}_{2'2} - \mathcal{D}_{2'233'} + \mathcal{D}_{33'2'22'2})\mathcal{D}_3\eta_{2'} + (1 - \mathcal{D}_{33'} - \mathcal{D}_{33'2'2} + \mathcal{D}_{2'233'33'})\mathcal{D}_{2'}\eta_3. \quad (\text{B2})$$

2. Sagnac variables

The three Sagnac variables α , β , and γ were proposed in [24]. First-generation α_1 reads

$$\alpha_1 = \eta_1 - \eta_{1'} + \mathcal{D}_3\eta_2 - \mathcal{D}_{2'1'}\eta_{2'} + \mathcal{D}_{31}\eta_3 - \mathcal{D}_{2'}\eta_{3'} , \quad (\text{B3})$$

while second-generation α_2 is given by

$$\begin{aligned} \alpha_2 = & (1 - \mathcal{D}_{2'1'3'})\eta_1 - (1 - \mathcal{D}_{312})\eta_{1'} + (1 - \mathcal{D}_{2'1'3'})\mathcal{D}_3\eta_2 \\ & - (1 - \mathcal{D}_{312})\mathcal{D}_{2'1'}\eta_{2'} + (1 - \mathcal{D}_{2'1'3'})\mathcal{D}_{31}\eta_3 - (1 - \mathcal{D}_{312})\mathcal{D}_{2'}\eta_{3'} . \end{aligned} \quad (\text{B4})$$

3. Fully symmetric variables

The fully symmetric combination ζ_1 [25] senses the constellation rotation, and combines all interferometric signals with exactly one delay

$$\zeta_1 = \mathcal{D}_1\eta_1 + \mathcal{D}_2\eta_2 + \mathcal{D}_3\eta_3 - \mathcal{D}_{1'}\eta_{1'} - \mathcal{D}_{2'}\eta_{2'} - \mathcal{D}_{3'}\eta_{3'} . \quad (\text{B5})$$

Due to its symmetry, there are no cyclic permutations of this variable. The second-generation version [6] is no longer fully symmetric under cyclic permutation of the indices, and reads

$$\begin{aligned} \zeta_2 = & (\mathcal{D}_{11'} - \mathcal{D}_{2'3'1'})\eta_1 + (\mathcal{D}_{1'2'} - \mathcal{D}_{322'})\eta_2 \\ & + (\mathcal{D}_{13} - \mathcal{D}_{2'3'3})\eta_3 - (\mathcal{D}_{1'1} - \mathcal{D}_{321})\eta_{1'} \\ & - (\mathcal{D}_{1'2'} - \mathcal{D}_{322'})\eta_{2'} - (\mathcal{D}_{13} - \mathcal{D}_{2'3'3})\eta_{3'} . \end{aligned} \quad (\text{B6})$$

4. Beacon, Monitor, and Relay

The Beacon P , Monitor E , and Relay U variables [6] can be used in the case of the failure of a link. The first generation reads

$$P_1 = -(\mathcal{D}_2 - \mathcal{D}_{3'1'})\eta_2 + (\mathcal{D}_2 - \mathcal{D}_{11'2})\eta_{2'} - (\mathcal{D}_{3'} - \mathcal{D}_{11'3'})\eta_3 + (\mathcal{D}_{3'} - \mathcal{D}_{21})\eta_{3'} , \quad (\text{B7})$$

$$E_1 = -(1 - \mathcal{D}_{11'})\eta_1 + (1 - \mathcal{D}_{11'})\eta_{1'} - (\mathcal{D}_3 - \mathcal{D}_{2'1'})\eta_2 + (\mathcal{D}_{2'} - \mathcal{D}_{31})\eta_{3'} , \quad (\text{B8})$$

$$U_1 = -(\mathcal{D}_{3'} - \mathcal{D}_{11'3'})\eta_{1'} + (1 - \mathcal{D}_{3'2'1'})\eta_2 - (1 - \mathcal{D}_{11'})\eta_{2'} + (\mathcal{D}_1 - \mathcal{D}_{3'2'})\eta_{3'} . \quad (\text{B9})$$

and their second generation is

$$\begin{aligned}
P_2 = & (\mathcal{D}_{3'22} - \mathcal{D}_{23'3'1'} - \mathcal{D}_{3'1'122} + \mathcal{D}_{211'3'3'1'})\eta_2 \\
& - (\mathcal{D}_{3'22} - \mathcal{D}_{3'2211'} - \mathcal{D}_{3'1'122} + \mathcal{D}_{3'1'12211'})\eta_{2'} \\
& + (\mathcal{D}_{23'3'} - \mathcal{D}_{23'3'1'1} - \mathcal{D}_{211'3'3'} + \mathcal{D}_{211'3'3'1'1})\eta_3 \\
& - (\mathcal{D}_{23'3'} - \mathcal{D}_{211'3'3'} - \mathcal{D}_{3'221} + \mathcal{D}_{3'1'1221})\eta_{3'} ,
\end{aligned} \tag{B10}$$

$$\begin{aligned}
E_2 = & -(1 - \mathcal{D}_{11'} - \mathcal{D}_{1'1} + \mathcal{D}_{11'1'1})\eta_1 \\
& + (1 - \mathcal{D}_{1'1} - \mathcal{D}_{11'} + \mathcal{D}_{1'111'})\eta_{1'} \\
& - (\mathcal{D}_3 - \mathcal{D}_{2'1'} - \mathcal{D}_{\bar{3}1'133} + \mathcal{D}_{\bar{2}'1'12'2'1'})\eta_2 \\
& + (\mathcal{D}_{2'} - \mathcal{D}_{31} - \mathcal{D}_{\bar{2}'1'12'2'} + \mathcal{D}_{\bar{3}1'1331})\eta_{3'} ,
\end{aligned} \tag{B11}$$

$$\begin{aligned}
U_2 = & -(\mathcal{D}_{13'} - \mathcal{D}_{11'3'2'3'} - \mathcal{D}_{111'3'} + \mathcal{D}_{3'2'1'111'3'})\eta_{1'} \\
& + (\mathcal{D}_1 - \mathcal{D}_{11'3'2'} - \mathcal{D}_{13'2'1'} + \mathcal{D}_{11'3'2'3'2'1'})\eta_2 \\
& - (\mathcal{D}_1 - \mathcal{D}_{111'} - \mathcal{D}_{11'3'2'} + \mathcal{D}_{3'2'1'111'})\eta_{2'} \\
& + (\mathcal{D}_{11} - \mathcal{D}_{13'2'} - \mathcal{D}_{3'2'1'11} + \mathcal{D}_{11'3'2'3'2'})\eta_{3'} .
\end{aligned} \tag{B12}$$

Appendix C: Clock correction for other TDI channels

We can apply the algorithm outlined in section IVD to find clock corrections for many, but not all TDI variables. For corrections to be exact, the delay polynomial P_i for each η_i have to be build out of pairs of delays corresponding to photon paths.

For some variables used in the literature, this requirement is too strict, and we do not find an exact correction. In most of these cases, we can still define a correcting expression assuming that delays commute. Such calibrations are not exact anymore, but it was shown in [18] that clock noise is still sufficiently suppressed.

Some of the delay polynomials do correspond to photon paths, but they start at the wrong spacecraft. In that case, we can extend the path to add another link to the correct spacecraft. This comes at the expense of an additional overall delay directly in front of the corresponding q_i . Since we can assume that delays commute, we can cancel this delay by applying a forward time shift to the whole expression.

1. Michelson variables

As discussed in section IVD 2, we find an exact clock-noise correcting expression for both generations. They read

$$\begin{aligned}
R_1 &= r_{1'} - \mathcal{D}_{2'}r_3 , \\
R_{1'} &= r_1 + \mathcal{D}_3r_{2'} , \\
R_2 &= 0 , \\
R_{2'} &= (1 - \mathcal{D}_{2'2})r_1 - r_{1'} - \mathcal{D}_{2'}r_3 , \\
R_3 &= r_1 - (1 + \mathcal{D}_{33'})r_{1'} - \mathcal{D}_3r_{2'} , \\
R_{3'} &= 0 ,
\end{aligned} \tag{C1}$$

for first generation and

$$\begin{aligned}
R_1 &= (1 - \mathcal{D}_{2'2})r_1 - (2 - \mathcal{D}_{33'} - \mathcal{D}_{33'2'2})r_{1'} \\
&\quad + (\mathcal{D}_3 - \mathcal{D}_{2'23})r_{2'} - (2\mathcal{D}_{2'} - \mathcal{D}_{33'2'} - \mathcal{D}_{33'2'22'})r_3, \\
R_{1'} &= (2 - \mathcal{D}_{2'2} - \mathcal{D}_{2'233'})r_1 - (1 - \mathcal{D}_{33'})r_{1'} \\
&\quad + (2\mathcal{D}_3 - \mathcal{D}_{2'23} - \mathcal{D}_{2'233'3})r_{2'} - (\mathcal{D}_{2'} - \mathcal{D}_{33'2'})r_3, \\
R_2 &= 0, \\
R_{2'} &= (2 - 2\mathcal{D}_{2'2} - \mathcal{D}_{2'233'} + \mathcal{D}_{33'2'22'})r_1 - (2 - \mathcal{D}_{33'} - \mathcal{D}_{33'2'2})r_{1'} \\
&\quad + (\mathcal{D}_3 - \mathcal{D}_{2'23})r_{2'} - (2\mathcal{D}_{2'} - \mathcal{D}_{33'2'} - \mathcal{D}_{33'2'22'})r_3, \\
R_3 &= (2 - \mathcal{D}_{2'2} - \mathcal{D}_{2'233'})r_1 - (2 - 2\mathcal{D}_{33'} - \mathcal{D}_{33'2'2} + \mathcal{D}_{2'233'33'})r_{1'} \\
&\quad + (2\mathcal{D}_3 - \mathcal{D}_{2'23} - \mathcal{D}_{2'233'3})r_{2'} - (\mathcal{D}_{2'} - \mathcal{D}_{33'2'})r_3, \\
R_{3'} &= 0,
\end{aligned} \tag{C2}$$

for the second generation.

2. Sagnac variables

Since each η only appears once in α_1 , we do not find any correcting expression. As discussed in section IV D 3, α_2 does satisfy our criterion for exact clock-noise correction, and the correcting terms are

$$\begin{aligned}
R_1 &= r_{1'} + \mathcal{D}_{2'1'}r_{2'} + \mathcal{D}_{2'}r_{3'}, \\
R_{1'} &= -r_1 - \mathcal{D}_3r_2 - \mathcal{D}_{31}r_3, \\
R_2 &= -(1 - \mathcal{D}_{2'1'3'})r_1 + r_{1'} + \mathcal{D}_{2'1'}r_{2'} + \mathcal{D}_{2'}r_{3'}, \\
R_{2'} &= -r_1 + (1 - \mathcal{D}_{312})r_{1'} - \mathcal{D}_3r_2 - \mathcal{D}_{31}r_3 + (\mathcal{D}_{2'} - \mathcal{D}_{3122'})r_{3'}, \\
R_3 &= -(1 - \mathcal{D}_{2'1'3'})r_1 + r_{1'} - (\mathcal{D}_3 - \mathcal{D}_{2'1'3'3})r_2 + \mathcal{D}_{2'1'}r_{2'} + \mathcal{D}_{2'}r_{3'}, \\
R_{3'} &= -r_1 + (1 - \mathcal{D}_{312})r_{1'} - \mathcal{D}_3r_2 - \mathcal{D}_{31}r_3.
\end{aligned} \tag{C3}$$

3. Fully symmetric Sagnac variables

Since each η_i only appears once in ζ_1 , we do not find any clock-noise correction for this TDI combination.

ζ_2 also does not satisfy our criterion for exact calibration, since *e.g.*, $\mathcal{D}_{11'} - \mathcal{D}_{3'2'1'}$ does not corresponds to an interferometer that starts at spacecraft 1. We can still define an approximate correcting expression, assuming that delays commute,

$$\begin{aligned}
R_1 &= r_{1'} - \mathcal{D}_{\bar{2}1'}r_2 + \mathcal{D}_{2'1'}r_{2'} + (\mathcal{D}_{\bar{2}} - \mathcal{D}_{\bar{2}1'1})r_3 + (\mathcal{D}_{2'} - \mathcal{D}_{\bar{2}})r_{3'}, \\
R_{1'} &= r_1 - (\mathcal{D}_3 - \mathcal{D}_{\bar{2}1'})r_2 - (\mathcal{D}_{\bar{2}} + \mathcal{D}_{31} - \mathcal{D}_{\bar{2}1'1})r_3 + \mathcal{D}_{\bar{2}}r_{3'}, \\
R_2 &= \mathcal{D}_{2'2}r_1 + \mathcal{D}_{2'}r_3 - \mathcal{D}_{2'}r_{3'}, \\
R_{2'} &= -\mathcal{D}_{2'2}r_1 - \mathcal{D}_{2'}r_3 + \mathcal{D}_{2'}r_{3'}, \\
R_3 &= \mathcal{D}_{33'}r_{1'} - \mathcal{D}_3r_2 + \mathcal{D}_3r_{2'}, \\
R_{3'} &= -\mathcal{D}_{33'}r_{1'} + \mathcal{D}_3r_2 - \mathcal{D}_3r_{2'}.
\end{aligned} \tag{C4}$$

4. Beacon, Monitor, and Relay

a. First generation

U_1 satisfies our criterion for an exact clock-noise correction. The corresponding correcting terms R_i are given by

$$\begin{aligned}
R_1 &= 0, \\
R_{1'} &= -r_2 + (1 - \mathcal{D}_{11'})r_{2'} - \mathcal{D}_1 r_{3'}, \\
R_2 &= +\mathcal{D}_{3'} r_{1'} + r_{2'} + \mathcal{D}_{3'2'} r_{3'}, \\
R_{2'} &= -r_2 - \mathcal{D}_1 r_{3'}, \\
R_3 &= 0, \\
R_{3'} &= \mathcal{D}_{3'} r_{1'} - r_2 + r_{2'}.
\end{aligned} \tag{C5}$$

E_1 does not satisfy our criterion for an exact clock-noise correction, since *e.g.* $1 - \mathcal{D}_{1'1}$ corresponds to an interferometer that does not start at spacecraft 1. We can still define an approximate correcting expression, assuming that delays commute,

$$\begin{aligned}
R_1 &= -\mathcal{D}_{\bar{3}'} r_2 + (\mathcal{D}_{\bar{3}'} - \mathcal{D}_{\bar{3}'11'}) r_{2'} - \mathcal{D}_{\bar{3}'1} r_{3'}, \\
R_{1'} &= \mathcal{D}_{\bar{2}1'} r_2 - (\mathcal{D}_{\bar{2}} - \mathcal{D}_{\bar{2}1'1}) r_3 + \mathcal{D}_{\bar{2}} r_{3'}, \\
R_2 &= r_1 - r_{1'} - \mathcal{D}_{2'} r_{3'}, \\
R_{2'} &= 0, \\
R_3 &= 0, \\
R_{3'} &= r_1 - r_{1'} + \mathcal{D}_3 r_2.
\end{aligned} \tag{C6}$$

P_1 does not satisfy our criterion for an exact clock-noise correction, since $\mathcal{D}_2 - \mathcal{D}_{11'2}$ corresponds to an interferometer that does not start at spacecraft 2. We can still define an approximate correcting expression, assuming that delays commute,

$$\begin{aligned}
R_1 &= 0, \\
R_{1'} &= 0, \\
R_2 &= (\mathcal{D}_{\bar{3}2} - \mathcal{D}_{\bar{3}1'3'}) r_1 - \mathcal{D}_{\bar{3}1'} r_{2'} + \mathcal{D}_{\bar{3}} r_3 - \mathcal{D}_{\bar{3}} r_{3'}, \\
R_{2'} &= \mathcal{D}_2 r_2 + \mathcal{D}_{21} r_{3'}, \\
R_3 &= -\mathcal{D}_{\bar{2}11'3'} r_{1'} - \mathcal{D}_{\bar{2}'} r_2 + (\mathcal{D}_{\bar{2}'} - \mathcal{D}_{\bar{2}'11'}) r_{2'} + (\mathcal{D}_{\bar{2}'3'} - \mathcal{D}_{\bar{2}'1} r_{3'}), \\
R_{3'} &= -(\mathcal{D}_{\bar{2}'3'} - \mathcal{D}_{\bar{2}'12}) r_{1'} + \mathcal{D}_{\bar{2}'} r_2 - \mathcal{D}_{\bar{2}'} r_{2'} + \mathcal{D}_{\bar{2}'1} r_3.
\end{aligned} \tag{C7}$$

b. Second generation

U_2 does not satisfy our criterion for an exact clock-noise correction. We can still define an approximate correcting expression, assuming that delays commute,

$$\begin{aligned}
R_1 &= 0, \\
R_{1'} &= -(\mathcal{D}_{13'} - \mathcal{D}_{111'3'})r_{1'} - (\mathcal{D}_{13'2'1'} - \mathcal{D}_{111'3'2'1'})r_{2'} - (\mathcal{D}_{13'2'} - \mathcal{D}_{111'3'2'})r_{3'}, \\
R_2 &= (\mathcal{D}_{13'} - \mathcal{D}_{11'3'2'3'})r_{1'} + (\mathcal{D}_1 - \mathcal{D}_{11'3'2'})r_{2'} + (\mathcal{D}_{13'2'} - \mathcal{D}_{11'3'2'3'2'})r_{3'}, \\
R_{2'} &= -(\mathcal{D}_{13'} - \mathcal{D}_{111'3'})r_{1'} - (\mathcal{D}_1 - \mathcal{D}_{111'})r_{2'} - (\mathcal{D}_{13'2'} - \mathcal{D}_{111'3'2'})r_{3'}, \\
R_3 &= 0, \\
R_{3'} &= (\mathcal{D}_{111'3'} - \mathcal{D}_{13'2'1'3'})r_{1'} + (\mathcal{D}_{111'} - \mathcal{D}_{13'2'1'})r_{2'} + (\mathcal{D}_{11} - \mathcal{D}_{13'2'})r_{3'}.
\end{aligned} \tag{C8}$$

E_2 does not satisfy our criterion for an exact clock-noise correction. We can still define an approximate correcting expression, assuming that delays commute,

$$\begin{aligned}
R_1 &= -(\mathcal{D}_{\bar{2}1'} - \mathcal{D}_{11'\bar{2}1'})r_2 + (\mathcal{D}_{\bar{2}} - \mathcal{D}_{\bar{2}1'1} - \mathcal{D}_{11'\bar{2}} + \mathcal{D}_{11'\bar{2}1'1})r_3 - (\mathcal{D}_{\bar{2}} - \mathcal{D}_{11'\bar{2}})r_{3'}, \\
R_{1'} &= (\mathcal{D}_{\bar{3}'} - \mathcal{D}_{1'1\bar{3}'})r_2 - (\mathcal{D}_{\bar{3}'} - \mathcal{D}_{\bar{3}'11'} - \mathcal{D}_{1'1\bar{3}'} + \mathcal{D}_{1'1\bar{3}'11'})r_{2'} + (\mathcal{D}_{\bar{3}'1} - \mathcal{D}_{1'1\bar{3}'1})r_{3'}, \\
R_2 &= -(\mathcal{D}_3 - \mathcal{D}_{2'1'})r_2 - (\mathcal{D}_{31} - \mathcal{D}_{2'1'1})r_{3'}, \\
R_{2'} &= 0, \\
R_3 &= 0, \\
R_{3'} &= +(\mathcal{D}_{2'} - \mathcal{D}_{31})r_{3'} + (\mathcal{D}_{2'1'} - \mathcal{D}_{311'})r_2.
\end{aligned} \tag{C9}$$

P_2 does not satisfy our criterion for an exact clock-noise calibration. We can still define an approximate calibrating expression, assuming that delays commute,

$$\begin{aligned}
R_1 &= 0, \\
R_{1'} &= 0, \\
R_2 &= (\mathcal{D}_{3'22} - \mathcal{D}_{23'3'1'})r_2 + (\mathcal{D}_{3'221} - \mathcal{D}_{23'3'1'1})r_{3'}, \\
R_{2'} &= -(\mathcal{D}_{3'22} - \mathcal{D}_{3'1'122})r_2 - (\mathcal{D}_{3'221} - \mathcal{D}_{3'1'1221})r_{3'}, \\
R_3 &= (\mathcal{D}_{23'3'1'} - \mathcal{D}_{211'3'3'1'})r_2 + (\mathcal{D}_{23'3'} - \mathcal{D}_{211'3'3'})r_{3'}, \\
R_{3'} &= -(\mathcal{D}_{23'3'1'} - \mathcal{D}_{3'2211'})r_2 - (\mathcal{D}_{23'3'} - \mathcal{D}_{3'221})r_{3'}.
\end{aligned} \tag{C10}$$

Appendix D: Flexing-filtering coupling in the corrected TDI variables

We give here the expressions of the residual clock-noise due to the flexing-filtering coupling in some corrected TDI variables. These residuals are given in the form of delay-filter commutators.

1. Michelson variables

We find for the first and second-generation Michelson variables,

$$X_1^{\mathcal{F},c} = b_{1'}(1 - \mathcal{D}_{33'})\mathcal{D}_{2'}[\mathcal{F}, \mathcal{D}_2]q_1 + a_1(1 - \mathcal{D}_{2'2})[\mathcal{F}, \mathcal{D}_3]q_2 + (b_{1'} - a_{1'})(1 - \mathcal{D}_{33'})[\mathcal{F}, \mathcal{D}_{2'}]q_3, \quad (\text{D1})$$

$$X_2^{\mathcal{F},c} = b_{1'}(1 - \mathcal{D}_{33'} - \mathcal{D}_{33'2'2} + \mathcal{D}_{2'233'33'})\mathcal{D}_{2'}[\mathcal{F}, \mathcal{D}_2]q_1 + a_1(1 - \mathcal{D}_{2'2} - \mathcal{D}_{2'233'} + \mathcal{D}_{33'2'22'})[\mathcal{F}, \mathcal{D}_3]q_2 + (b_{1'} - a_{1'})(1 - \mathcal{D}_{33'} - \mathcal{D}_{33'2'2} + \mathcal{D}_{2'233'33'})[\mathcal{F}, \mathcal{D}_{2'}]q_3. \quad (\text{D2})$$

2. Sagnac variables

We find for the second-generation Sagnac variable,

$$\alpha_2^{\mathcal{F},c} = b_{1'}(1 - \mathcal{D}_{2'1'3'})\mathcal{D}_{31}[\mathcal{F}, \mathcal{D}_2]q_1 - a_1(1 - \mathcal{D}_{2'1'3'})[\mathcal{F}, \mathcal{D}_3]q_2 + (a_{2'} - b_{2'})(1 - \mathcal{D}_{312})\mathcal{D}_{2'}[\mathcal{F}, \mathcal{D}_{1'}]q_2 + (a_{1'} - b_{1'})(1 - \mathcal{D}_{312})[\mathcal{F}, \mathcal{D}_{2'}]q_3 - (a_3 + b_{1'} + b_{3'})(1 - \mathcal{D}_{2'1'3'})\mathcal{D}_3[\mathcal{F}, \mathcal{D}_1]q_3. \quad (\text{D3})$$

ACKNOWLEDGMENTS

We gratefully acknowledge support by the Deutsches Zentrum für Luft- und Raumfahrt (DLR, German Space Agency) with funding from the Federal Ministry for Economic Affairs and Energy based on a resolution of the German Bundestag (Project Ref. No. 500Q1601 and 500Q1801). This research has been sup-

ported by the Centre National d'Études Spatiales (CNES), the CNRS, the Université Paris-Diderot, as well as the NASA Postdoctoral Fellowship program. The development of `LISANode` is part of the LISA Simulation Group activities. We are also grateful to the members of the LISA Simulation Group for their comments and help in improving the manuscript. In particular, we thank G. Heinzel, A. Petiteau and M. Tinto for the fruitful discussions regarding this topic.

-
- [1] P. Amaro-Seoane *et al.* (LISA Collaboration), *Laser Interferometer Space Antenna*, Tech. Rep. (ESA, 2017) arXiv.org:1702.00786 [astro-ph].
 - [2] M. Armano *et al.*, Phys. Rev. Lett. **116**, 231101 (2016).
 - [3] M. Armano *et al.*, Phys. Rev. Lett. **120**, 061101 (2018).
 - [4] M. Otto, *Time-Delay Interferometry Simulations for the Laser Interferometer Space Antenna*, Ph.D. thesis, Gottfried Wilhelm Leibniz Universität Hannover (2015).
 - [5] M. Tinto and J. W. Armstrong, Phys. Rev. D **59**, 102003 (1999).
 - [6] M. Tinto, F. B. Estabrook, and J. W. Armstrong, Phys. Rev. **D69**, 082001 (2004), arXiv:gr-qc/0310017 [gr-qc].
 - [7] G. de Vine, B. Ware, K. McKenzie, R. E. Spero, W. M. Klipstein, and D. A. Shaddock, Phys. Rev. Lett. **104**, 211103 (2010), arXiv:1005.2176 [astro-ph.IM].
 - [8] T. Schwarze, G. Fernández Barranco, D. Penkert, O. Gerberding, G. Heinzel, and K. Danzmann, J. Phys. Conf. Ser. **716**, 012004 (2016).

- [9] M. Laporte, H. Halloin, E. Bréelle, C. Buy, P. Grüning, and P. Prat, *J. Phys. Conf. Ser.* **840**, 012014 (2017).
- [10] R. Cruz, J. Thorpe, M. Hartman, and G. Mueller, *AIP Conf. Proc.* **873**, 319 (2006).
- [11] M. Vallisneri, *Phys. Rev. D* **71**, 022001 (2005), arXiv:gr-qc/0407102.
- [12] A. Petiteau, G. Auger, H. Halloin, O. Jeanin, E. Plagnol, S. Pireaux, T. Regimbau, and J.-Y. Vinet, *Phys. Rev. D* **77**, 023002 (2008), arXiv:0802.2023 [gr-qc].
- [13] J.-B. Bayle, M. Lilley, A. Petiteau, and H. Halloin, *Phys. Rev. D* **99**, 084023 (2019), arXiv:1811.01575 [astro-ph.IM].
- [14] LISA Science Study Team, *LISA Science Requirements Document*, Tech. Rep. 1.0 (ESA, 2018) <https://www.cosmos.esa.int/web/lisa/lisa-documents/>.
- [15] G. Weaver, J. Garstecki, and S. Reynolds, in *42nd Annual Precise Time and Time Interval (PTTI) Systems and Applications Meeting 2010* (2010) pp. 369–379.
- [16] Y. Wang, *On inter-satellite laser ranging, clock synchronization and gravitational wave data analysis*, Ph.D. thesis, Gottfried Wilhelm Leibniz Universität Hannover (2017).
- [17] S. Barke, *Inter-Spacecraft Frequency Distribution for Future Gravitational Wave Observatories*, Ph.D. thesis, Gottfried Wilhelm Leibniz Universität Hannover (2015).
- [18] M. Tinto and O. Hartwig, *Phys. Rev. D* **98**, 042003 (2018).
- [19] R. W. Hellings, *Phys. Rev. D* **64**, 022002 (2001), arXiv:gr-qc/0012013 [gr-qc].
- [20] M. Vallisneri, *Phys. Rev. D* **72**, 042003 (2005), [Erratum: *Phys. Rev. D* **76**, 109903 (2007)], arXiv:gr-qc/0504145 [gr-qc].
- [21] K. Rajesh Nayak, S. Koshti, S. V. Dhurandhar, and J.-Y. Vinet, *Class. Quant. Grav.* **23**, 1763 (2006).
- [22] B. Chauvineau, T. Regimbau, J.-Y. Vinet, and S. Pireaux, *Phys. Rev. D* **72**, 122003 (2005), arXiv:gr-qc/0511157 [gr-qc].
- [23] S. Plaszczynski, *Fluct. Noise Lett.* **7**, R1 (2007), arXiv.org:0510081 [astro-ph].
- [24] M. Tinto, F. B. Estabrook, and J. W. Armstrong, *Phys. Rev. D* **65**, 082003 (2002).
- [25] J. W. Armstrong, F. B. Estabrook, and M. Tinto, *The Astrophysical Journal* **527**, 814 (1999).